Communications

Magnetic Properties

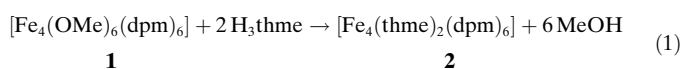# Energy-Barrier Enhancement by Ligand Substitution in Tetrairon(III) Single-Molecule Magnets[**]

Andrea Cornia,* Antonio C. Fabretti, Pierfrancesco Garrisi, Cecilia Mortalò, Daniele Bonacchi, Dante Gatteschi, Roberta Sessoli, Lorenzo Sorace, Wolfgang Wernsdorfer, and Anne-Laure Barra

The tailoring of the structure and properties of single-molecule magnets (SMMs) is a very active branch of

[*] Dr. A. Cornia, Prof. Dr. A. C. Fabretti, P. Garrisi, C. Mortalò
Dipartimento di Chimica—Centro SCS
Università di Modena e Reggio Emilia, UdR INSTM
Via G. Campi 183, 41100 Modena (Italy)
Fax: (+39) 059-373543
E-mail: acornia@unimore.it

D. Bonacchi, Prof. Dr. D. Gatteschi, Prof. Dr. R. Sessoli
Dipartimento di Chimica
Università di Firenze, UdR INSTM
Polo scientifico universitario, via della Lastruccia 3
50019 Sesto Fiorentino (Italy)

Dr. W. Wernsdorfer
Laboratoire Louis Néel-CNRS
BP166, 25 Avenue des Martyrs
38042 Grenoble Cedex 9 (France)

Dr. L. Sorace, Dr. A.-L. Barra
Laboratoire des Champs Magnetiques Intenses-CNRS
BP166, 25 Avenue des Martyrs
38042 Grenoble Cedex 9 (France)

modern coordination chemistry. Investigations on classes of structurally related SMMs, such as those of the Mn_{12} family, have helped unravel the mechanisms underlying slow magnetic relaxation in high-spin molecules, a key step in both fundamental and application-oriented research.[1] At the same time, the search for new SMMs with higher blocking temperatures has fueled synthetic efforts aimed, on one side, at increasing structural control on cluster architectures[2] and, on the other side, at developing the so-called serendipitous-assembly approach.[3] An elegant strategy for structural design is based on site-specific modification of preformed clusters.[4] Carboxylate abstraction from Mn_{12} clusters, for instance, has been carried out site specifically using a variety of incoming ligands, such as nitrates,[4a] phosphanates,[4b] phosphates,[4c] or different carboxylates.[4d] However, these substitutions are accompanied by only small perturbation of the magnetic properties.

The SMM behavior is associated with the magnetic anisotropy of clusters, which in turn depends on local anisotropies and on the way they vectorially add to give a resulting total anisotropy.[5a] Herein we show that site-specific ligand replacement provides a means to raise the symmetry of Fe_4 clusters from C_2 to D_3, which results in a dramatic increase of magnetic anisotropy and energy barrier. Fe_4 clusters are among the simplest inorganic systems showing SMM behavior.[5,6] The archetypal member of this class is the tetrairon(III) compound $[Fe_4(OMe)_6(dpm)_6]$ (**1**) (Hdpm = dipivaloylmethane). The six μ-methoxide ligands bridge a central iron(III) ion to three peripheral iron centers arranged at the vertices of an isosceles triangle[5a] with a crystallographic C_2 symmetry, and some disorder which yields three different isomers in the lattice. At low temperature, the cluster has a high-spin state ($S = 5$) and an easy-axis magnetic anisotropy, two requisites for the observation of slow magnetic relaxation. For the major component, the second-order zero-field splitting (ZFS) parameters are $D = -0.206(1)$ cm^{-1} and $E = 0.010(3)$ cm^{-1}. In addition, the presence of sizeable fourth-order contributions has been demonstrated.[5b]

To eliminate the lattice disorder, we attempted to replace the methoxide bridges in **1** with a tripodal ligand, 1,1,1-tris(hydroxymethyl)ethane (H_3thme), which affords facial coordination in octahedral iron(III) complexes [Eq. (1)].[7]

$$[Fe_4(OMe)_6(dpm)_6] + 2\,H_3thme \rightarrow [Fe_4(thme)_2(dpm)_6] + 6\,MeOH \qquad (1)$$
$$\mathbf{1} \qquad\qquad\qquad\qquad\qquad \mathbf{2}$$

The new tetrairon(III) cluster **2** (see Experimental Section) crystallizes in a highly ordered trigonal lattice and exhibits an enhanced SMM behavior compared with **1**.

The molecular structure of **2**, as revealed by a single-crystal X-ray study at 100(2) K, has crystallographic D_3 symmetry (Figure 1). The C_3 axis passes through Fe1, C2, and C3, whereas the three C_2 axes are directed along Fe1···Fe2, Fe1···Fe2′ and Fe1···Fe2″. As a consequence, the Fe_4 moiety is perfectly planar and the six alkoxide bridges are crystallographically equivalent to each other. The main structural differences between **1** and **2** directly reflect the geometric constraints imposed by the thme^{3-} ligand. In particular, the ligand "bite" reduces the O1-Fe1-O1′ angle
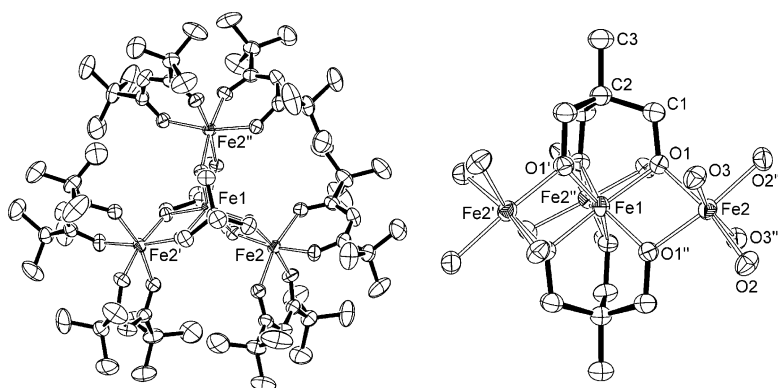
DOI: 10.1002/anie.200352989

Figure 1. ORTEP[17c] representation of the molecular structure of **2** viewed slightly off the trigonal axis (left) and perpendicular to it (right; only the Fe/O framework and the thme^{3-} ligands are shown). Thermal ellipsoids are set at 50% probability and hydrogen atoms have been omitted for clarity. Selected interatomic distances [Å] and angles [°]: Fe1···Fe2 3.0858(4), Fe2···Fe2′ 5.3448(7), Fe1-O1 1.9810(12), Fe2-O1 1.9639(12); Fe1-O1-Fe2 102.92(5), O1-Fe1-O1′ 89.16(5), O1-Fe1-O1″ 76.68(7), O1-Fe2-O1″ 77.47(7).

(89.16(5) versus 93.6°), which leads to a shorter Fe1···Fe2 separation (3.0857(3) versus 3.137 Å).

The temperature dependence of the molar magnetic susceptibility (Figure 2) is characteristic of antiferromagnetic
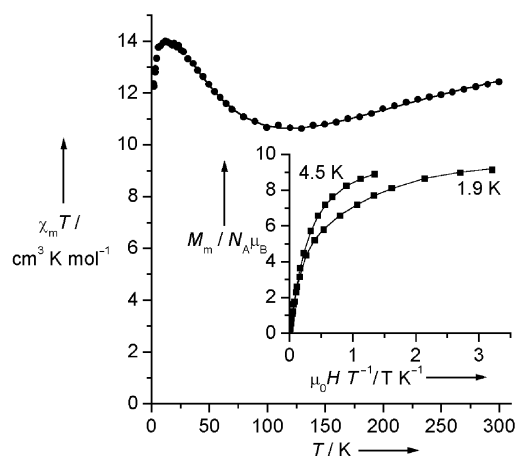
fitted using an axial ZFS Hamiltonian with $D = -0.42(1)$ cm^{-1} and $S = 5$. To further support these conclusions, variable-temperature high-frequency EPR (HF-EPR) spectra have been recorded at 190 and 230 GHz. In the 190 GHz spectrum at 10 K (Figure 3) two sets of EPR signals arising from the transitions with magnetic field parallel and perpendicular to the symmetry axis are clearly visible in the low- and high-field regions, respectively. The largest extension of the spectrum is observed at low field and the lines in the parallel set gain intensity with decreasing field, a clear indication of a large spin ground state and a negative D parameter. In fact, when the energy quantum of the microwave radiation (≈ 9 K at 190 GHz) is comparable with the thermal energy, the $M_S = -4 \leftarrow -5$ signal has the strongest intensity owing to the enhanced population of the $M_S = -5$ state. The spectra can be accurately reproduced with $S = 5$, $g = 2.00$, and $D = -0.445$ cm^{-1}, in good agreement with the magnetization data. To our knowledge, compound **2** has the largest D value so far reported for an iron(III)-based SMM.

Figure 2. $\chi_m T$ versus T and M_m versus $\mu_0 H/T$ plots for a powder sample of **2**, along with best-fit calculated data (solid lines).
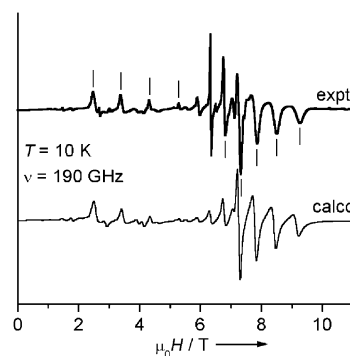

Figure 3. Experimental and simulated HF-EPR powder spectra of **2** at 10 K and 190 GHz. The pattern of signals discussed in the text is marked with vertical lines.

clusters with incomplete spin cancellation. The fitting of susceptibility data gives $J_1 = 16.51(8)$ cm^{-1} (antiferromagnetic) and $J_2 = -0.62(8)$ cm^{-1} (ferromagnetic) for the nearest-neighbor and next-nearest-neighbor Heisenberg constants, respectively. J_1 is significantly smaller in **2** than in **1** ($J_1 = 21.1$ cm^{-1}), consistent with the smaller Fe-O-Fe angle subtended by the alkoxide bridges (102.92(5) versus 104.3°).[5a]

The occurrence of an $S = 5$ ground spin state, expected to afford a $\chi_m T$ value close to 15 cm^3 K mol^{-1} at low temperature, is confirmed by molar magnetization versus field data at 4.5 and 1.9 K (Figure 2 inset), which approach the appropriate saturation value $M_m = 10 N_A \mu_B$ in high fields. The detailed field dependence at both temperatures can be accurately

The twofold increase of the $|D|$ parameter following site-specific ligand substitution demonstrates the subtle structural dependence of magnetic anisotropy in iron(III) clusters. Two main terms associated with dipole–dipole interactions and single-ion anisotropies need to be considered.[8] Dipolar interactions contribute -0.034 and -0.036 cm^{-1} to the ground state D parameter of **1** and **2**, respectively, the difference being due to the slightly shorter Fe···Fe separation in the latter.[5a, 9] Arguably, the large D variation in the two compounds has to be ascribed to different single-ion terms, which are known to be very sensitive to structural distortions. Angular-overlap model (AOM) calculations have previously been used to analyze the effect of trigonal compression and rotation on the magnetic anisotropy of a FeO$_6$ chromophore (the two types of distortions are measured by the angles θ and ϕ, whose values are 54.74° and 60°, respectively, in a regular octahedron[10,11]). The results show that trigonal compression

leads to a positive single-ion D value (elongation to a negative value), while rotation of an octahedral face along the threefold axis favors a negative D value.[5a, 10] The central iron(III) ion Fe1 shows a larger extent of trigonal rotation in **2** ($\phi = 29.2°$) than in **1** ($\phi = 41.8°$). Moreover, trigonal compression occurs in **1** ($\theta = 57.3°$), whereas slight elongation is observed in **2** ($\theta = 54.1°$). Hence, the AOM predicts a greater tendency of the Fe1 spin in **2** to lie along the unique molecular axis, which leads to an enhanced easy-axis anisotropy in the $S = 5$ ground state of the cluster.

AC and DC susceptibility measurements with the polarizing magnetic field directed along the c axis have been used to study the temperature dependence of the magnetic relaxation time τ in zero field (Figure 4). In the high-
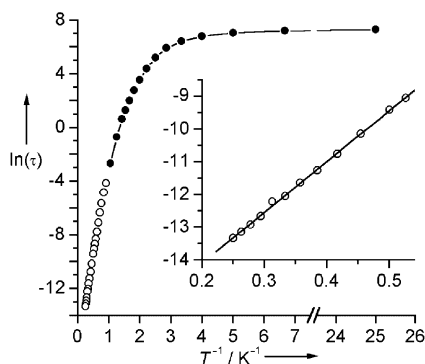
Figure 4. Magnetic relaxation time measured on a single crystal of **2** by DC (●) and AC (○) techniques (the solid line is a guide to the eye). The inset shows the high-temperature region along with the best-fit line.

temperature limit, $\ln(\tau)$ varies linearly with $1/T$ as predicted by the Arrhenius law.[1] A linear fit of the data at $T \geq 1.9$ K gives thermal activation parameters $U_{\mathrm{eff}}/k_B = 15.6(2)$ K and $\tau_0 = 3.4(2) \times 10^{-8}$ s. In contrast, τ approaches a temperature-independent value of approximately 1500 s below 0.2 K, a clear signature of quantum tunneling (QT) within the ground $M_S = \pm 5$ doublet. U_{eff} represents the actual barrier to be overcome for the reversal of the magnetization and its value is found to be very close to the energy gap between the $M_S = 0$ and $M_S = \pm 5$ states, $U/k_B = (|D|/k_B)S^2 = 16.0$ K (11.1 cm^{-1}). This result indicates that barrier short-cuts by QT are rather ineffective. By contrast, U_{eff} in compound **1** was found to be significantly smaller than U (3.5 versus 7.4 K).[5a] The difference can be qualitatively explained recalling that barrier short-cuts are activated by transverse anisotropies.[1,12] A dominant role is played by second-order terms, which are present in **1** but are forbidden in **2** because of its strictly axial symmetry. Fourth-order terms are also expected to be rather ineffective in **2** because for trigonal symmetry they can promote tunneling only between states whose M_S values differ by multiples of ± 3,[1] that is, only within the excited $M_S = \pm 3$ doublet in absence of external field.

Hysteresis loops on single crystals of **2** have also been recorded (Figure 5). Abrupt variations of the magnetization occur at regular field intervals $\Delta(\mu_0H) = D/g\,\mu_B \cong 0.5$ T, that is, whenever the applied fields brings energy levels of the zero-
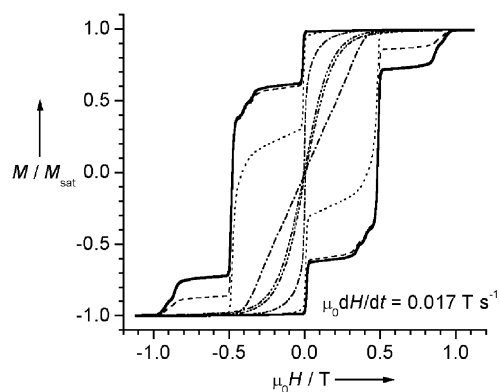
Figure 5. Hysteresis loops recorded on a single crystal of **2** with a field sweep rate of 0.017 Ts^{-1} and at different temperatures: 0.04 to 0.2 K (——), 0.4 K (-----), 0.6 K (•••••), 0.8 K (–•–•), and 1.15 K (----). The magnetic field has been applied along the crystallographic c axis.

field split multiplet into coincidence.[1] Spin–spin cross relaxation may contribute to the fine structure of the $M_S = 4 \leftarrow -5$ and $M_S = 3 \leftarrow -5$ transitions around 0.5 and 1.0 T.[13] Below around 0.2 K the relaxation becomes temperature independent, which shows that it occurs purely by a QT mechanism.

In conclusion, site-specific ligand replacement heavily affects the ground-state anisotropy of Fe$_4$ SMMs and, in addition, provides a simple way to control molecular symmetry and tunneling mechanisms. We are now applying the same technique for the functionalization of Fe$_4$ clusters with surface-binding groups that may promote the formation of ordered molecular adsorbates on solid supports.[14]

Experimental Section

All chemicals were used as received, except for methanol which was dried by distillation over Mg(OMe)$_2$ before use. NaOMe was used as a 2.96 M solution in methanol, freshly prepared by careful addition of sodium metal to anhydrous methanol under inert atmosphere.

1: The compound was obtained by a variation on the reported synthesis.[5a, 15] The dimer [Fe$_2$(OMe)$_2$(dpm)$_4$] (**3**) was prepared as described by Rossman and co-workers by reaction of resublimed FeCl$_3$ with Hdpm in anhydrous methanol, but replacing piperidine with sodium methoxide.[16] Resublimed FeCl$_3$ (0.119 g, 0.735 mmol) was added to a stirred suspension of **3** (1.00 g, 1.10 mmol) in MeOH/Et$_2$O 1:2 v/v (93 mL) to give a deep red solution, and then NaOMe (0.75 mL, 2.22 mmol) was added. The yellow mixture was stirred for 40 min and diluted with MeOH/Et$_2$O 1:4 v/v (312 mL). After additional 15 min stirring, NaCl was removed by gooch filtration (G4) and the resulting yellow solution was divided into five 80-mL portions. Slow diffusion of methanol vapors (100 mL) into each portion over 2 weeks gave yellow rod-like crystals of **1** in 60–65 % yield. Elemental analysis calcd (%) for C$_{72}$H$_{132}$O$_{18}$Fe$_4$: C 57.30, H 8.82; found: C 57.75, H 9.13.

2: Compound **1** (0.180 g, 0.12 mmol) was dissolved in dry Et$_2$O (75 mL) and treated with H$_3$thme (0.035 g, 0.29 mmol). Slow diffusion of methanol vapors (75 mL) into the filtered solution over 4–5 days gave yellow prisms of **2** in 70–75 % yield. Elemental analysis calcd (%) for C$_{76}$H$_{132}$O$_{18}$Fe$_4$: C 58.62, H 8.54; found: C 58.49, H 8.55. MS (D.I.P., 70 eV): m/z (%): 1557 (<1) [M^+], 1374 (7) [M^+–dpm], 850 (50), 768 (5), 651 (6), 595 (12), 545 (10), 535 (5), 422 (100) [Fe(dpm)$_2^+$], 365 (59), 239 (29) [Fe(dpm)$^+$], 127 (7).

Crystal structure data for **2**: $C_{76}H_{132}O_{18}Fe_4$, $M_r = 1557.22$, crystal dimensions $0.28 \times 0.23 \times 0.21$ mm, trigonal, space group $R\bar{3}c$, $a = 16.1893(12)$, $c = 56.712(10)$ Å, $V = 12873(3)$ Å^3, $Z = 6$, $\rho_{calcd} = 1.205$ g cm^{-3}, $2\theta_{max} = 56.56°$, Mo$_{K\alpha}$ radiation, $\lambda = 0.71073$ Å, $T = 100(2)$ K. Of the 33070 reflections collected on a BRUKER X8APEX system, 3564 were independent and were used in the structure refinement (Lorentz, polarization and absorption corrections applied, $\mu = 0.723$ mm^{-1}, min./max. transmission $= 0.8233/0.8631$). The structure was solved by direct methods using BRUKER-SHELXTL-V6.12 package and refined on F_o^2 using SHELXL-97 program[17a] implemented in the WINGX suite.[17b] One *tert*-butyl group was found to be disordered over two positions with 0.849(5) and 0.151(5) occupancies, respectively. All non-hydrogen atoms were refined anisotropically, except for the methyl carbon atoms of the disordered *t*Bu group in the lower-occupancy position. Hydrogen atoms were added in idealized positions, with torsion angle refinement for Me groups. The values of R1 and wR2 are 0.0370 [$I > 2\sigma(I)$] and 0.1089 (all data) for 172 parameters and 7 restraints. The maximum and minimum residual electron density are 0.454 and -0.285 e Å^{-3}, respectively. CCDC-220804 (**2**) contains the supplementary crystallographic data for this paper. These data can be obtained free of charge via www.ccdc.cam.ac.uk/conts/retrieving.html (or from the Cambridge Crystallographic Data Centre, 12 Union Road, Cambridge CB21EZ, UK; fax: $(+44)1223$-336-033; or deposit@ccdc.cam.ac.uk).

HF-EPR spectra of **2** were recorded on a home-build spectrometer equipped with two Gunn oscillators working at fundamental frequencies of 95 and 115 GHz respectively, with double and triple harmonic generator at the Grenoble High Magnetic Field Laboratory. The sample was pressed in a pellet to prevent preferential orientation of the crystallites. Simulations of HF-EPR spectra were obtained by full diagonalization of the spin Hamiltonian matrix, using an already described calculation procedure.[18] Magnetic data on microcrystalline powder samples have been recorded using a Cryogenic S600 SQUID magnetometer, with applied fields of 0.1 T (for $T \leq 50$ K) and 1 T (for $T > 50$ K) in susceptibility versus T measurements. The diamagnetic contribution of the sample was estimated from Pascal's constants and subtracted from the data. Low-temperature magnetic measurements on single crystals were performed using an array of micro-SQUIDS.[19] Measurements were performed on this magnetometer in the temperature range 0.035–7.0 K, with fields up to 1.4 T. The field can be applied in any direction by separately driving three orthogonal coils. AC susceptibility measurements on single crystals of the order of 0.1 mm were performed with a home-built Hall probe magnetometer. It works in the temperature range between 30 mK and 30 K, for frequencies between 1 Hz and 1 MHz, and for applied fields up to 1.4 T. The field can be applied in any direction with a precision better than 0.1°.

[1] D. Gatteschi, R. Sessoli, *Angew. Chem.* **2003**, *115*, 278; *Angew. Chem. Int. Ed.* **2003**, *42*, 268, and references therein.
[2] G. L. Abbati, A. Caneschi, A. Cornia, A. C. Fabretti, Y. A. Pozdniakova, O. I. Shchegolikhina, *Angew. Chem.* **2002**, *114*, 4699; *Angew. Chem. Int. Ed.* **2002**, *41*, 4517.
[3] R. E. P. Winpenny, *J. Chem. Soc. Dalton Trans.* **2002**, 1.
[4] a) P. Artus, C. Boskovic, J. Yoo, W. E. Streib, L.-C. Brunel, D. N. Hendrickson, G. Christou, *Inorg. Chem.* **2001**, *40*, 4199; b) C. Boskovic, M. Pink, J. C. Huffman, D. N. Hendrickson, G. Christou, *J. Am. Chem. Soc.* **2001**, *123*, 9914; c) T. Kuroda-Sowa, S. Fukuda, S. Miyoshi, M. Maekawa, M. Munakata, H. Miyasaka, M. Yamashita, *Chem. Lett.* **2002**, 682; d) M. Soler, P.

Artus, K. Folting, J. C. Huffman, D. N. Hendrickson, G. Christou, *Inorg. Chem.* **2001**, *40*, 4902.
[5] a) A. L. Barra, A. Caneschi, A. Cornia, F. Fabrizi de Biani, D. Gatteschi, C. Sangregorio, R. Sessoli, L. Sorace, *J. Am. Chem. Soc.* **1999**, *121*, 5302; b) A. Bouwen, A. Caneschi, D. Gatteschi, E. Goovaerts, D. Schoemaker, L. Sorace, M. Stefan, *J. Phys. Chem. B* **2001**, *105*, 2658.
[6] R. W. Saalfrank, I. Bernt, M. M. Chowdhry, F. Hampel, G. B. M. Vaughan, *Chem. Eur. J.* **2001**, *7*, 2765.
[7] A. Cornia, D. Gatteschi, K. Hegetschweiler, L. Hausherr-Primo, V. Gramlich, *Inorg. Chem.* **1996**, *35*, 4414, and references therein.
[8] G. L. Abbati, L.-C. Brunel, H. Casalta, A. Cornia, A. C. Fabretti, D. Gatteschi, A. K. Hassan, A. G. M. Jansen, A. L. Maniero, L. Pardi, C. Paulsen, U. Segre, *Chem. Eur. J.* **2001**, *7*, 1796.
[9] D. Gatteschi, R. Sessoli, A. Cornia, *Chem. Commun.* **2000**, 725.
[10] D. Gatteschi, L. Sorace, *J. Solid State Chem.* **2001**, *159*, 253.
[11] E. L. Muetterties, L. J. Guggenberger, *J. Am. Chem. Soc.* **1974**, *96*, 1748.
[12] A. L. Barra, D. Gatteschi, R. Sessoli, *Chem. Eur. J.* **2000**, *6*, 1608.
[13] W. Wernsdorfer, S. Bhaduri, R. Tiron, D. N. Hendrickson, G. Christou, *Phys. Rev. Lett.* **2002**, *89*, 197201.
[14] A. Cornia, A. C. Fabretti, M. Pacchioni, L. Zobbi, D. Bonacchi, A. Caneschi, D. Gatteschi, R. Biagi, U. Del Pennino, V. De Renzi, L. Gurevich, H. S. J. Van der Zant, *Angew. Chem.* **2003**, *115*, 1683; *Angew. Chem. Int. Ed.* **2003**, *42*, 1645.
[15] G. Amoretti, S. Carretta, R. Caciuffo, H. Casalta, A. Cornia, M. Affronte, D. Gatteschi, *Phys. Rev. B* **2001**, *64*, 104403.
[16] C.-H. S. Wu, G. R. Rossman, H. B. Gray, G. S. Hammond, H. J. Schugar, *Inorg. Chem.* **1972**, *11*, 990.
[17] a) G. M. Sheldrick, SHELXL-97, Program for Crystal Structure Refinement (Release 97–2), Institüt für Anorganische Chemie der Universität, Göttingen, Germany, **1998**; b) L. J. Farrugia, *J. Appl. Crystallogr.* **1999**, *32*, 837; c) L. J. Farrugia, *J. Appl. Crystallogr.* **1997**, *30*, 565.
[18] C. J. H. Jacobsen, E. Pedersen, J. Villadsen, H. Weihe, *Inorg. Chem.* **1993**, *32*, 1216.
[19] W. Wernsdorfer, *Adv. Chem. Phys.* **2001**, *118*, 99.